Published in final edited form as:
Nature. 2016 September 8; 537(7619): 210–213. doi:10.1038/nature19315.

Massive radius-dependent flow slippage in carbon nanotubes

Eleonora Secchi[1], **Sophie Marbach**[1], **Antoine Niguès**[1], **Derek Stein**[1,2], **Alessandro Siria**[1,*], and **Lydéric Bocquet**[1,*]

[1]Laboratoire de Physique Statistique, Ecole Normale Supérieure, PSL Research University,75005 Paris Cedex 05, France

[2]Physics Department, Brown University, Providence, RI, 02912, USA

Abstract

Simulations and measurements have established that water moves through carbon nanotubes with exceptionally high rates due to nearly frictionless interfaces1–4. These observations have stimulated interest in nanotube-based membranes for applications that range from desalination to nano-filtration and energy harvesting5–10, yet the exact water transport mechanisms inside the nanotubes and at the water-carbon interface continue to be controversially discussed11,12 because existing theories fail to provide a satisfying explanation for the limited number of experimental results available to date13. This is because even though controlled and systematic studies have explored transport through individual nanotubes8,9,14–7, none has met the considerable technical challenge of unambiguously measuring the permeability of a single nanotube11. Here we show that the pressure-driven flow rate across individual nanotubes can be determined with unprecedented sensitivity and without dyes from the hydrodynamics of water jets as they emerge from single nanotubes into a surrounding fluid. Our measurements reveal unexpectedly large and radius-dependent surface slippage in carbon nanotubes (CNT), and no slippage in boron-nitride nanotubes (BNNT) that are crystallographically similar to CNTs but differ electronically. This pronounced contrast between the two systems must originate from subtle differences in atomic-scale details of their solid-liquid interfaces, strikingly illustrating that nanofluidics is the frontier where the continuum picture of fluid mechanics confronts the atomic nature of matter.

Measuring the pressure-driven flow of water through individual CNTs and BNNTs with well-defined radii (R_t) and lengths (L_t) requires overcoming two significant challenges. First, the flow rate through a tube drops too precipitously for even state-of-the-art flow rate measurements to detect when R_t decreases down to the nanoscale. Flow rates as low as a few

*Correspondence and requests for materials should be addressed to L.B. (lyderic.bocquet@lps.ens.fr) and A.S. (alessandro.siria@lps.ens.fr).

Author Information

Author information Reprints and permissions information is available at www.nature.com/reprints.

The authors declare no competing financial interests.

Author Statement: L.B. and A.S. conceived and directed the research. A.N. and A.S. designed and fabricated the nanotube devices. E.S and D.S. designed the fluidic cell. E.S. performed the measurements. The data were analyzed by E.S., S.M. and L.B.; S.M. conducted the numerical analysis with input from the other authors. All authors contributed to the scientific discussions and the preparation of the manuscript.

Europe PMC Funders Author Manuscripts

pL/s have been measured across single nanocapillaries [18], but that is still about three orders of magnitude higher than the sensitivity required to probe mass flow across a single nanotube. Our approach avoids this problem by focusing instead on the flow that a fluid jet entrains outside a nanotube (see Fig. 1) and the peculiar scaling property of the jet hydrodynamics [19]: the external flow is characterized by a driving force F_P that originates in the fluid momentum transfer at the tube opening [20, 21] and scales linearly with R_t, so the flow velocities remain measurably large even when R_t shrinks to nanoscopic dimensions. The second challenge is fabricating an experimental system for manipulating and using a single nanotube, in the form of a nanofluidic needle with a single nanotube protruding from the tip. To do this, we adapted our recently developed technique for selecting and manipulating nanotubes of known length and diameter with a nanomanipulator operating inside a scanning electron microscope (SEM) [9]; see Supplementary Methods 1, and Supplementary Video. We guided a nanotube into the tip of a laser-pulled glass nanocapillary with an orifice in the range 250-350 nm. The dimensions of the nanotubes were determined by ionic transport measurements and by electron microscopy (see Supplementary Methods 2 and 4). For this study we tested five different CNTs with dimensions (R_t, L_t) = (15,700), (17,450), (33,900), (38,800), and (50,1000) (in nm) and three different BNNTs with dimensions (R_t, L_t) = (23,600), (26,700) and (7,1300) (in nm); see Supplementary Methods 2 and 4 and Supplementary Table 1.

The nanotube at the tip of the glass capillary bridged two macroscopic fluid reservoirs: one inside the capillary and another in the wide, transparent flow cell into which the capillary was placed (see Fig. 1(b) and Supplementary Methods 3). We filled both reservoirs with potassium chloride (KCl) solutions of a chosen concentration C_s and controlled pH, and seeded the flow cell with 500 nm polystyrene tracer particles. We then applied a pressure drop ΔP to the capillary and tracked the resulting motion of the tracers under a microscope (see Fig. 1(b)) in order to map the velocity profile of the flow (see Fig. 1(c) and 2). Flow measurements were performed with salt concentration $C_s=10^{-3}$ M or $C_s=10^{-2}$ M. Low salinity is required during the tracking experiments to prevent salt-induced colloid aggregation.

Ag/AgCl electrodes inserted into either reservoir were used to measure the ionic conductance across the nanotube before and after each fluidic experiment to ensure the integrity of the device, as well as to obtain information on the dimensions and the surface charge density of the nanotube (see Supplementary Methods 4). These electrodes were grounded during flow measurements.

Due to the needle geometry of the system, the pressure-driven flow through the nanotube sets up a flow in the outer reservoir called a Landau-Squire (LS) nanojet [18, 20, 21]. The LS solution of the Navier-Stokes equations at low Reynolds number predicts radial and angular components of the flow velocity equal to $v_r=\frac{F_P}{4\pi\eta}\frac{\cos\theta}{r}$ and $v_\theta=-\frac{F_P}{8\pi\eta}\frac{\sin\theta}{r}$, respectively, where r is the radial distance from the tip, θ is the angle relative to the jet's symmetry axis, and η is the viscosity [20]. F_P is the driving force of the jet applied at the origin. Fig. 2(a)-(b) show that our measurements of the flow field around single nanotubes fully agree with the LS prediction. The inset of Fig. 2(b) further highlights the long-range $1/r$

dependence of the LS flow, which remarkably extends over tens of micrometres despite the nanoscopic size of the flow's source.

From our analysis of the LS flow, we extracted experimental values of F_P for every nanotube and each ΔP. The results, presented in Fig. 2(c), show a linear relationship between F_P and ΔP. To gain insight into the permeability of the nanotubes, we begin by observing that the mass flow rate and F_P are both proportional to ΔP, hence proportional to one another. The viscous origin of F_P at low Reynolds numbers and dimensional considerations motivate the definition $F_P = \alpha \eta R_t v_{NT}$, where $\alpha \sim O(1)$ is a geometry-dependent numerical prefactor and v_{NT} is the average fluid velocity inside the nanotube. The permeability of the tube k_{NT} is defined by $v_{NT} = \frac{k_{NT}}{\eta} \frac{\Delta P}{L_t}$. Combining these expressions, F_P, k_{NT}, and ΔP are related by

$$F_P(\Delta P) = \frac{\alpha R_t k_{NT}}{L_t} \times \Delta P \quad (1)$$

According to Eq.(1), the slope of the plots in Fig. 2(c) provides an estimate of the nanotube permeability, so we can already see that the permeability of CNTs is greatly enhanced as compared with BNNTs. But in order to properly quantify the permeabilities, we need to know the value of α. We calculated α from the precise relationship between F_P, v_{NT}, and ΔP that we obtained by solving numerically the full hydrodynamic LS flow in detail. Furthermore, since α might be sensitive to details of the geometry of the nanotube and the tip, we repeated our calculations for every nanotube device based on its particular geometry, as measured by SEM (see Supplementary Methods 6). This exhaustive study, which combines numerical hydrodynamic calculations with experimental benchmarking using nanocapillaries, is summarized in the Supplementary Methods 5. Our study showed that $\alpha \approx 0.3$ for the nanotube devices considered in Fig. 2(a)-(b), with only small variations between nanotubes. Having removed all uncertainty from the value of α, we could obtain accurate values for k_{NT} from the experimental dependence of F_P on ΔP. Figure 3(a) presents the dependence of k_{NT} on R_t for every nanotube. The permeabilities are normalized by a simple no-slip reference, $k_{no-slip}^{ref} = R_t^2/8$, corresponding to a nanotube of the same size with a no-slip boundary condition at its surface. Note that the flow from the smallest BNNT tube with R_t = 7 nm was below the detection limit.

We attribute the enhanced permeability of the CNTs to hydrodynamic slippage at the carbon surface [12, 13, 22, 23]. The fundamental way to account for this is to introduce a slip length b and apply Navier's slip boundary condition to the fluid at the nanotube surface. We included the slip condition in our numerical analysis of the hydrodynamics of each nanotube device and obtained experimental b values by matching the computed flow rate enhancement due to surface slippage with the measured permeability data in Fig. 3(a) (see Supplementary Methods 6). This analysis, which uses the geometry of each nanotube device and takes into account hydrodynamic entrance effects at the nanotube ends, offers the most accurate estimation of b possible. We note that the permeability and b can also be quantitatively obtained from an analytical model of hydrodynamic resistances in series, using the Sampson

formula to account for both Poiseuille flow with slippage inside the nanotube and entrance effects [24]; see Supplementary Tables 2 and 3.

The peculiar nature of the water-carbon interface inside CNTs is revealed in Fig.3(b), which presents the experimentally determined slip length as a function of R_t. A first key observation is that the slip length is strongly radius-dependent, reaching 300 nm inside the smallest CNT investigated here. Interestingly, this observation allows us to resolve a long-standing debate surrounding the large difference in permeabilities reported previously in separate studies [2, 3, 4, 25] using large-scale CNT membranes. The results of those studies are consistent with a decreasing permeability enhancement factor for larger nanotubes, and the range of slip lengths they reported is fairly compatible with what we have measured. This also explains why the slip lengths measured previously inside CNTs were consistently much larger than the values measured on planar hydrophobic surfaces [13], where b is typically a few tens of nanometres at most. From a theoretical perspective, the transport behaviour of water inside CNTs has been the subject of numerous studies, mostly using molecular dynamics (MD) simulations [12,13]. Radius-dependent slippage was predicted inside CNTs with $R_t < 10$ nm [22, 23] and rationalized in terms of curvature-dependent friction [23]. The results presented here confirm the predicted trend, but the measured slip lengths far exceed the numerical predictions. This suggests that MD simulations do not represent the interfacial dynamics well at a quantitative level, echoing similar limitations encountered in studies of slippage at hydrophobic surfaces [13].

A second key feature of Fig. 3(c) is the vastly different behaviour of CNTs and BNNTs, with the latter showing no significant slippage of water at all. The comparison is illuminating because CNTs and BNNTs have the same crystallography but radically different electronic properties, with CNTs being semi-metallic and BNNTs insulating. That these nearly identical channels exhibit strongly different surface flow dynamics is unexpected, with MD simulations using semi-empirical interfacial parameters predicting in fact rather similar flow behaviour across CNTs and BNNTs [28, 29]. More recent ab-initio simulations predict that the friction of water on carbon surfaces is lower than on boron-nitride surfaces [30], but even these predictions strongly underestimate the profound difference observed here. The stark differences in flow behaviour must thus originate in subtle atomic-scale details of the solid-liquid interface, including the electronic structure of the confining material. More detailed understanding will require a systematic theoretical investigation of physico-chemical factors which could possibly affect surface friction, *e.g.* chemical surface dissociation, specific ion adsorption, etc. Useful information could also be gained by measuring the slip behaviour in CNT at high salt concentrations, a regime where the surface charge of CNTs is expected to increase [15].

In closing, we note that the unexpected slippage behaviour inside CNTs and BNNTs points to a hereto not appreciated link between hydrodynamic flow and surface properties of the confining material that opens an interesting new avenue for research bridging the gap between hard and soft condensed matter physics. In terms of the method we have developed, we expect that with further improvements in sensitivity it will enable the direct measurement of water transport across biological channels such as aquaporins.

Europe PMC Funders Author Manuscripts

Supplementary Material

Refer to Web version on PubMed Central for supplementary material.

Acknowledgements

L.B. and A.S. thank U. Keyser for many fruitful discussions. E.S., A.N., S.M. and A.S. acknowledge funding from the European Union's H2020 Framework Programme / ERC Starting Grant agreement number 637748 - NanoSOFT. L.B. and D.S. acknowledge support from the European Union's FP7 Framework Programme / ERC Advanced Grant Micromegas. S.M. acknowledges funding from a J.-P. Aguilar grant. L.B. acknoweldges funding from a PSL chair of excellence. Authors acknowledge funding from ANR project BlueEnergy.

References

[1]. Hummer G, Rasaiah JC, Noworyta JP. Water conduction through the hydrophobic channel of a carbon nanotube. Nature. 2001; 414:188–190. [PubMed: 11700553]

[2]. Majumder M, Chopra N, Andrews R, Hinds BJ. Nanoscale hydrodynamics enhanced flow in carbon nanotubes. Nature. 2005; 438:44. [PubMed: 16267546]

[3]. Holt JK, et al. Fast mass transport through sub-2-nanometer carbon nanotubes. Science. 2006; 312:1034–1037. [PubMed: 16709781]

[4]. Whitby M, Cagnon L, Thanou M, Quirke MN. Enhanced Fluid Flow through Nanoscale Carbon Pipes. Nano Lett. 2008; 8:2632–2637. [PubMed: 18680352]

[5]. Nair RR, Wu HA, Jayaram PN, Grigorieva IV, Geim AK. Unimpeded permeation of water through helium-leak-tight graphene-based membranes. Science. 2012; 335:442–444. [PubMed: 22282806]

[6]. Joshi RK, Carbone P, Wang FC, Kravets VG, Su Y, Grigorieva IV, Wu HA, Geim AK, Nair RR. Precise and Ultrafast Molecular Sieving Through Graphene Oxide Membranes. Science. 2014; 343:752–754. [PubMed: 24531966]

[7]. Park HG, Jung Y. Carbon nanofluidics of rapid water transport for energy applications. Chem Soc Rev. 2014; 43:565–576. [PubMed: 24141359]

[8]. Liu H, et al. Translocation of single stranded DNA through single-walled carbon nanotubes. Science. 2010; 327:64–67. [PubMed: 20044570]

[9]. Siria A, Poncharal P, Biance AL, Fulcrand R, Blase X, Purcel ST, Bocquet L. Giant osmotic energy conversion measured in a single transmembrane boron nitride Nanotube. Nature. 2013; 494:455–458. [PubMed: 23446417]

[10]. Geng J, et al. Stochastic transport through carbon nanotubes in lipid bilayers and live cell membranes. Nature. 2014; 514:612–615. [PubMed: 25355362]

[11]. Guo S, Meshot ER, Kuykendall T, Cabrini S, Fornasiero F. Nanofluidic Transport through Isolated Carbon Nanotube Channels: Advances, Controversies, and Challenges. Adv Mater. 2015; 27:5726–5737. [PubMed: 26037895]

[12]. Whitby M, Quirke N. Fluid flow in carbon nanotubes and nanopipes. Nat Nanotechnol. 2007; 2:87–94. [PubMed: 18654225]

[13]. Bocquet L, Charlaix E. Nanofluidics, from bulk to interfaces. Chem Soc Rev. 2010; 39:1073–1095. [PubMed: 20179826]

[14]. Lee CY, Choi W, Han J-H, Strano MS. Coherence Resonance in a Single-Walled Carbon Nanotube Ion Channel. Science. 2010; 329:1320. [PubMed: 20829480]

[15]. Secchi E, Nigués A, Jubin L, Siria A, Bocquet L. Scaling behavior for ionic transport and its fluctuations in individual carbon nanotubes. Phys Rev Lett. 2016; 116:154501. [PubMed: 27127970]

[16]. Qin X, Yuan Q, Zhao Y, Xie S, Liu Z. Measurement of the Rate of Water Translocation through Carbon Nanotubes. Nano Lett. 2011; 11:2173–2177. [PubMed: 21462938]

[17]. Lorenz U, Zewail A. Observing liquid ow in nanotubes by 4D electron microscopy. Science. 2014; 344:1496–1500. [PubMed: 24970082]

[18]. Laohakunakorn N, et al. A Landau-Squire Nanojet. Nano Lett. 2013; 13:5141–5146. [PubMed: 24124664]

[19]. Eggers J, Villermaux E. Physics of Liquid Jets. Rep Prog Phys. 2008; 71:036601.

[20]. Landau, LD.; Lifshitz, EM. Fluid mechanics, Vol. 6 of Course of Theoretical Physics. Pergamon; London: 1959.

[21]. Squire HB. The round laminar jet. J Mech Appl Math. 1951; 4:321–329.

[22]. Thomas JA, McGaughey AJH. Reassessing fast water transport through carbon nanotubes. Nano Lett. 2008; 8:2788–2793. [PubMed: 18665654]

[23]. Falk K, Sedlmeier F, Joly L, Netz RR, Bocquet L. Molecular Origin of Fast Water Transport in Carbon Nanotube Membranes: Superlubricity versus Curvature Dependent Friction. Nano Lett. 2010; 10:4067–4073. [PubMed: 20845964]

[24]. Sampson RA. On Stokes' current function. Phil Trans Roy Soc. 1891; A 182:449–518.

[25]. Mattia D, Leese H, Lee KP. Carbon nanotube membranes: From ow enhancement to permeability. Journal of Membrane Science. 2015; 475:266–272.

[26]. Maali A, Cohen-Bouhacina T, Kellay H. Measurement of the slip length of water flow on graphite surface. App Phys Lett. 2008; 92:053101.

[27]. Joseph S, Aluru NR. Why are carbon nanotubes fast transporters of water? Nano Lett. 2008; 8:452–458. [PubMed: 18189436]

[28]. Suk ME, Raghunathan AV, Aluru NR. Fast reverse osmosis using boron nitride and carbon nanotubes. Appl Phys Lett. 2008; 92:133120.

[29]. Hilder TA, Gordon D, Chung S-H. Salt Rejection and Water Transport Through Boron Nitride Nanotubes. Small. 2009; 5:2183–2190. [PubMed: 19582727]

[30]. Tocci G, Joly L, Michaelides A. Friction of Water on Graphene and Hexagonal Boron Nitride from Ab Initio Methods: Very Different Slippage Despite Very Similar Interface Structures. Nano Lett. 2014; 14:6872–6877. [PubMed: 25394228]

Europe PMC Funders Author Manuscripts

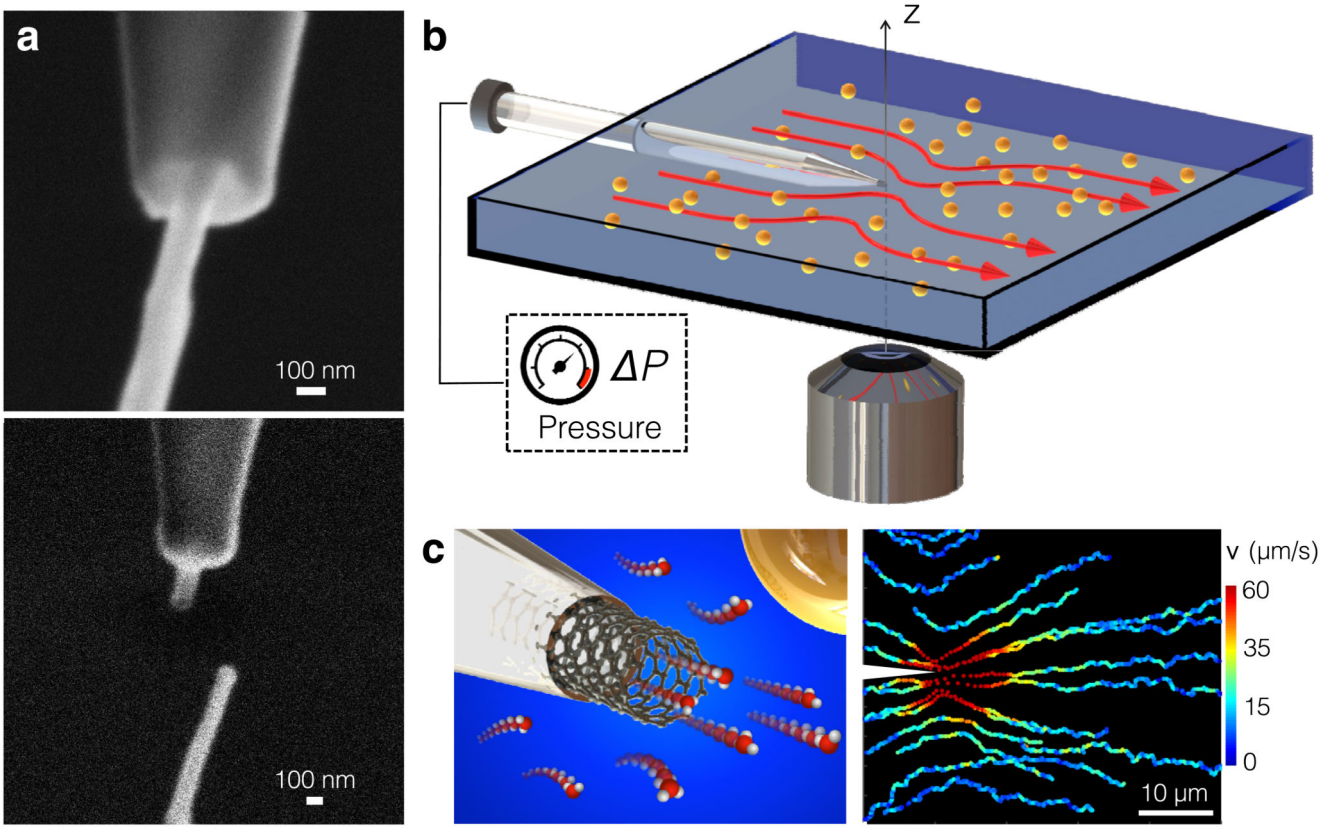

Figure 1. Nanojet experimental set-up

(a) SEM image of a CNT insertion into a nanocapillary (top) and after sealing (bottom). The CNT has dimensions (R_t, L_t)=(50,1000) nm. **(b)** Sketch of the fluidic cell used to image the Landau-Squire flow set-up by nanojets emerging from individual nanotubes. **(c)** (Left) Sketch of a nanotube protruding from a nanocapillary tip. (Right) Trajectories of individual colloidal tracers in a Landau-Squire flow field in the outer reservoir. The flow was driven by a nanojet from a CNT whose dimensions were (R_t, L_t) =(33,900) nm, with ΔP=1.7 bar. Both reservoirs contained water with 10^{-2} M KCl.

Europe PMC Funders Author Manuscripts

Europe PMC Funders Author Manuscripts

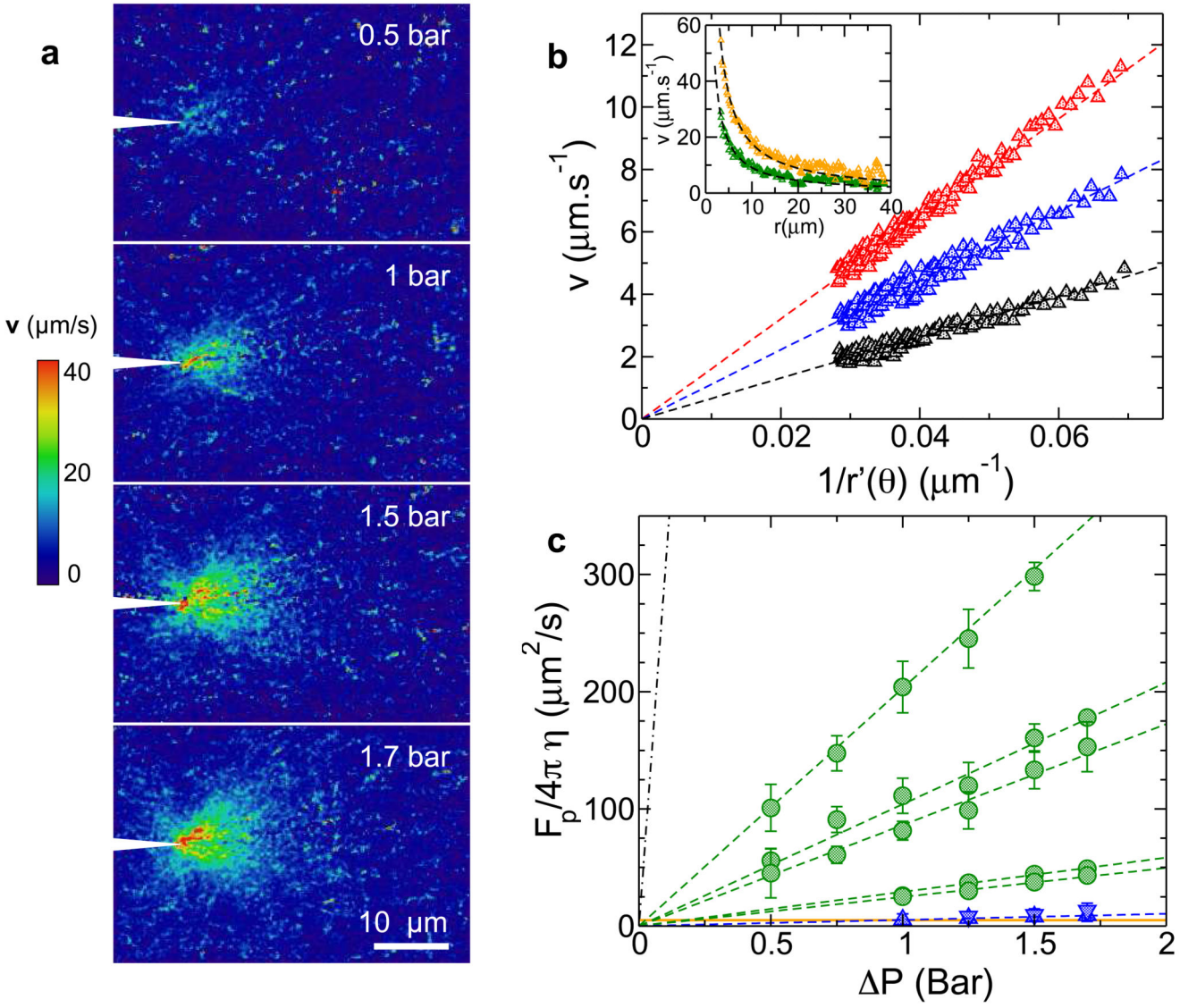

Figure 2. Measurement of Landau-Squire flows driven from nanotubes

(a) Maps of the velocity field near a CNT with (R_t, L_t) =(33, 900) nm for various ΔP (C_s=10^{-2} *M* and pH 6). **(b)** Magnitude of mean particle velocity as a function of $r'(\theta)=r\times 2/\sqrt{1+3cos^2\theta}$ for *ΔP*=0.5, 1, and 1.5 bar (from bottom to top). Dashed lines are fits of the Landau-Squire prediction. Inset: Particle velocity along the jet axis (θ = 0) versus distance from the nanotube for *ΔP*=0.75 bar (green) and *ΔP*=1.7 bar (orange). The dashed line is a 1/*r* fit. **(c)** ΔP -dependence of $\frac{F_P}{4\pi\eta}$ for CNTs (green symbols) and BNNTs (blue symbols). CNT dimensions were, from top to bottom, (R_t, L_t) = (50,1000) nm, (33,900) nm, (38,800) nm, (15,700) nm, and (17,450) nm and BNNT (R_t, L_t) = (26,700) nm and (23,600) nm. The salt concentration is C_s=10^{-3} *M*, except for the 33 nm CNT which was studied at both C_s=10^{-3} *M* and C_s=10^{-2} *M* without a detectable difference. Dashed green lines are linear fits from which the permeability was calculated. The orange line indicates the lowest

detectable flow strength. The black dashed line corresponds to the results of a control experiment using a nanocapillary without a nanotube (see Supplementary Method 5). Error bars correspond to the uncertainty in the slope in panel (b), estimated from at least 3 measurement replicates at each ΔP.

Europe PMC Funders Author Manuscripts

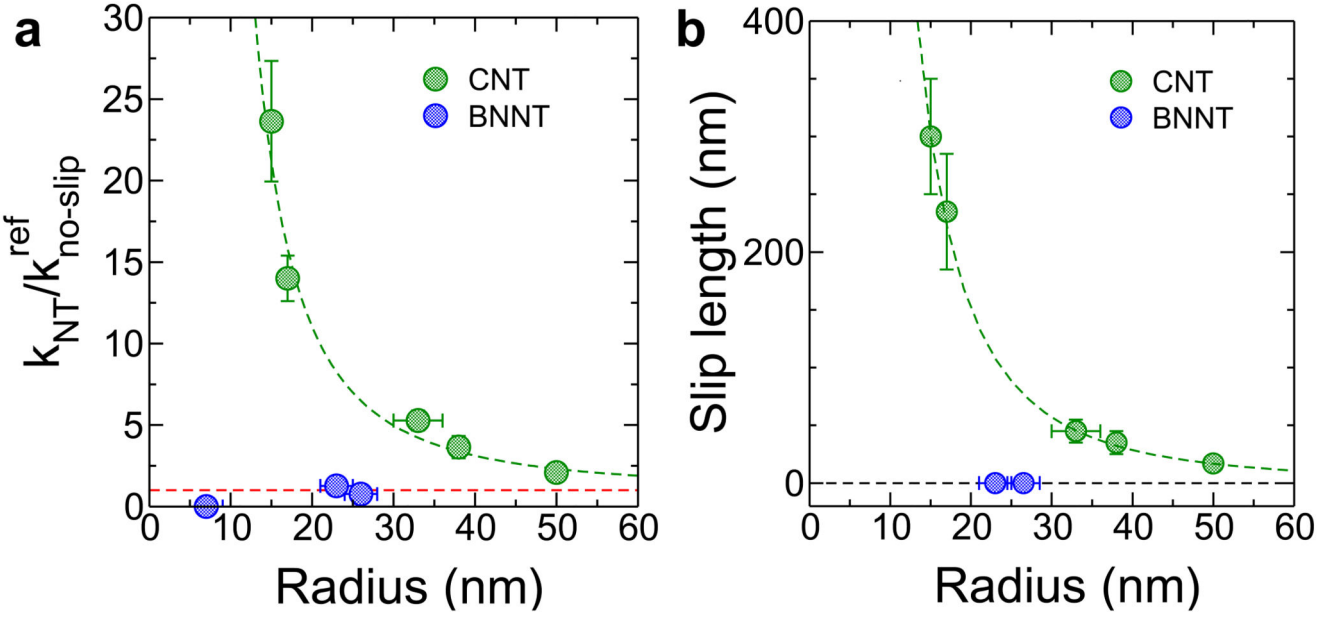

Figure 3. Permeability and slip length of individual CNTs and BNNTs

(a) Normalized permeability $(k_{\mathrm{NT}}/k^{ref}_{no-slip})$ of CNTs (green symbols) and BNNTs (blue symbols) as a function of R_t. The permeability of the R_t =7 nm BNNT was below the experimental detection limit and is indicated as k_{NT} = 0 for completeness. Error bars correspond to the experimental errors on F_P. **(b)** R_t dependence of the experimentally determined slip length inside CNTs (green) and BNNTs (blue). Error bars correspond to the uncertainty in the permeability. Salt concentration is C_s=10^{-3} *M*, except for the 33 nm CNT which was studied at both C_s=10^{-3} *M* and C_s=10^{-2} *M* without a detectable difference. In (a) and (b), the horizontal dashed line indicates the no-slip prediction $(k_{\mathrm{NT}}/k^{ref}_{no-slip})$=1 and the green dashed line is a guide to the eye. The error bars on the radius correspond to the experimental uncertainty in the electric characteristics (see Supplementary Methods 2 and 4). The values of the slip lengths are reported in Supplementary Tables 2 and 3.